Appl. Phys. A (2015) 121:1219–1226
DOI 10.1007/s00339-015-9493-5

Applied Physics A
Materials Science & Processing

Pulse laser deposition fabricated InP/Al-ZnO heterojunction solar cells with efficiency enhanced by an i-ZnO interlayer

Qiong Nian[1] · Kyle H. Montgomery[2] · Xin Zhao[2] · Tom Jackson[3] · Jerry M. Woodall[2] · Gary J. Cheng[1]

Received: 13 August 2015 / Accepted: 11 September 2015 / Published online: 22 September 2015

Abstract Indium phosphide (InP) has long since been seen as the ideal material choice for single-junction solar cells given its optimal band gap and high absorption coefficient. We report on the performance of heterojunction solar cells formed by depositing aluminum-doped ZnO (AZO), using pulsed laser deposition for the first time, onto p-type InP substrates. It is also found that a ZnO insulator layer (i-ZnO) between an InP base and AZO emitter can yield higher solar conversion efficiency and quantum efficiency over a baseline AZO/InP device. This 10-nm-thick intrinsic ultra-thin buffer enhanced collection probability but decreased surface recombination rate, which in turn shoot short-circuit current, open-circuit voltage, and fill factor to 17.4 mA/cm^2, 0.58 V, and 72.9 %, respectively. A maximum power conversion efficiency of 7.3 % was realized by intergrading i-ZnO, which is $\sim$20 % higher than baseline AZO/InP device of 6.1 %. This is also the record for this type of cell structure, using AZO as the emitter.

Qiong Nian and Kyle H. Montgomery have contributed equally to this work.

✉ Jerry M. Woodall
jwoodall@ucdavis.edu

✉ Gary J. Cheng
gjcheng@purdue.edu

[1] School of Industrial Engineering, Purdue University, West Lafayette, IN 47907, USA

[2] Department of Electrical and Computer Engineering, University of California, Davis, CA 95616, USA

[3] Department of Electrical Engineering, The Pennsylvania State University, University Park, PA 16802, USA

1 Introduction

Ongoing work in the field of solar photovoltaics primarily centers on either increasing cell efficiency with minimal increase in production cost or reducing production costs while maintaining cell efficiency. A corresponding shift by either approach results in lower cost per energy yield, commonly denoted by the dollar per watt ($/W) metric. While a variety of semiconductor materials have been used for producing solar cells, indium phosphide (InP) is closest to the ideal for a single-junction solar cell in terms of its band gap and absorption coefficient. With a band gap (E_g) of 1.33 eV, a theoretical efficiency of 33.5 % could be reached, which is the maximum for a single-junction cell, assuming detailed balance [1]. Additionally, with an absorption coefficient [2, 3] of $\sim 10^5$ cm^{-1}, InP can absorb >90 % of all photons with energies greater than E_g in slightly over 2 μm of material. Further, InP is resilient against radiation bombardment and has been used extensively in space power applications [4]. However, on the downside, InP has traditionally been too expensive to commercialize on a large scale using bulk substrates.

This work is focused on investigating a method of producing single-junction InP-based solar cells. To fabricate InP-based heterojunction solar cells, indium tin oxide (ITO) on InP has been studied extensively in the past as the emitter [5–12], but diffusion of tin into the p-type InP substrates resulted in a buried homojunction and was difficult to control. Alternatively, zinc oxide (ZnO) was studied to a lesser degree, but has many benefits including high conductivity and high transparency at visible wavelengths. Previous investigations focused on ZnO deposited by reactive sputtering, which resulted in a damaged interface and limited device performance [11, 13]. Prior to this work, Pande and Manikopoulos achieve the best

performance of ZnO–InP heterojunction solar cell with an efficiency of 6.6 % under AM 1 illumination [14]. Their work also utilized an InP base grown by vapor-phase epitaxy. In this work, we revisit the use of ZnO as alternative transparent conductive oxide (TCO) to form a heterojunction to InP substrates, with a specific focus on investigating the effect of a pure i-ZnO deposition between aluminum-doped ZnO (AZO) emitter and InP base. Though other epitaxial growth of oxide on InP has been used like magnetron sputtering [15], pulse laser deposition (PLD) has not been explored to deposit AZO and ZnO onto p-type InP substrates. The enlightening use of i-ZnO could trace to prior advancements of thin film solar cell efficiency improved by tuning conduction band offset and thus avoiding carrier recombination and open-circuit voltage loss [10, 16, 17].

2 Experimental details

In the current study, PLD was used to deposit AZO and i-ZnO onto p-type InP substrates for the first time. A commercial zinc-doped InP substrate ($N_A \approx 3 \times 10^{17}$ - cm^{-3}) was used. Individual samples were diced from a larger substrate prior to processing. The substrates were cleaned with acetone followed by isopropanol in an ultrasonic cleaner. Immediately prior to metal evaporation, each substrate was chemically etched using H_2SO_4:H_2O_2:H_2O (3:1:1) for 30 s, followed by rinse in deionized water and nitrogen (N_2) drying. Au/Zn/Au (30/45/120 nm) contacts were thermally evaporated onto the back side of the InP substrates followed by annealing at 450 °C for 30 s. Next, each substrate was etched again in H_2SO_4:H_2O_2:H_2O (3:1:1) for 30 s, followed by HCl:H_2O (1:5) for 1 m, followed by rinse in deionized water and N_2 drying. This was used to remove the native oxide and any damage due to the annealing. Finally, the cleaned substrates were immediately loaded into PLD chamber. The PLD chamber was pumped down for 12 h ($\sim 10^{-6}$ T) before starting the deposition process to remove impurity gas. Then, oxygen was introduced to the chamber to reach the pressure of 1 mT as the deposition condition. Finally, an AZO thin film was deposited onto the front side of the InP substrates ("baseline" sample) using a sintered ceramic 2 wt% Al AZO target at room temperature. A 248 nm excimer laser fluence of 0.5 J/cm^2 and a repetition rate of 5 Hz were applied during the deposition. A total AZO thickness of 150 nm was deposited. For the sample denoted "with i-ZnO," a 10-nm intrinsic ZnO layer was deposited prior to AZO layer using an intrinsic ZnO target. The deposition conditions of 150 mT oxygen pressure, 1.5 J/cm^2 laser fluence, and 10 Hz repetition rate were used for i-ZnO layer. The higher oxygen pressure of i-ZnO deposition compared to the AZO deposition is attributed to the requirement of intrinsic ZnO layer formation. After the PLD, standard photolithography processes were used to define an aluminum grid on the front surface (on top of AZO layer), whose details are described as follows: (1) photoresist spin coating, (2) exposure and development, (3) aluminum evaporation by e-beam, (4) lift-off in acetone. Mesa isolation was completed using an Acetic:H_3PO_4:H_2O (1:1:30) etch for 30 s followed by rinse and N_2 blow dry. Schematic overviews of the device structures are given in Fig. 1a. Mesa area for each device was 0.0625 cm^2 with a total grid area representing 12 % of the mesa area.

3 Results and discussions

3.1 Band structure

Comparing these two device schemes in Fig. 1a, the thin intrinsic ZnO layer utilized as a buffer layer might be able to increase the shunt resistance [18] and reduce the impact of randomly occurring electrical shunt paths in the device [10, 19]. Since according to prior statements, the local series resistance provided by the i-ZnO prevents electrical inhomogeneities like sites of locally enhanced recombination, from dominating the open-circuit voltage of the entire device [20, 21]. In turn, this could result in a positive influence on open-circuit voltage [10, 22]. Therefore, to fill the gap, we explored the effects of an i-ZnO interlayer between an InP base and AZO emitter on the external quantum efficiency (EQE), internal quantum efficiency (IQE), and conversion efficiency. Prior to full device characterization, due to surface states, the Fermi level in InP has been shown to be pinned close to the conduction band [23], necessitating the use of p-type InP with a TCO having a work function close to the electron affinity of InP. The band alignments between ZnO (or AZO) and InP are favorable in this regard. Figure 1b shows the alignments between InP and AZO, as well as an equilibrium band diagram. These diagrams assume a Schottky model and use an electron affinity of 4.4 eV for InP [24], a work function of 4.08 eV for AZO [25], and band gaps of 1.35 and 3.92 eV for InP and AZO [26], respectively. It deserves to note that a conduction band offset of $\Delta E_C = 0.18$ eV was formed in the equilibrium band alignments between InP and AZO. However, as shown in Fig. 1c, with i-ZnO between InP and AZO, the conduction band offset will be enlarged to $\Delta E_C = 0.30$ eV according to a working function of 4.60 eV [27] for i-ZnO and an energy difference of 0.50 eV between Fermi level and conduction band [28]. Referring to conversion efficiency as a function of this type of conduction band offset in prior advancement [29], the

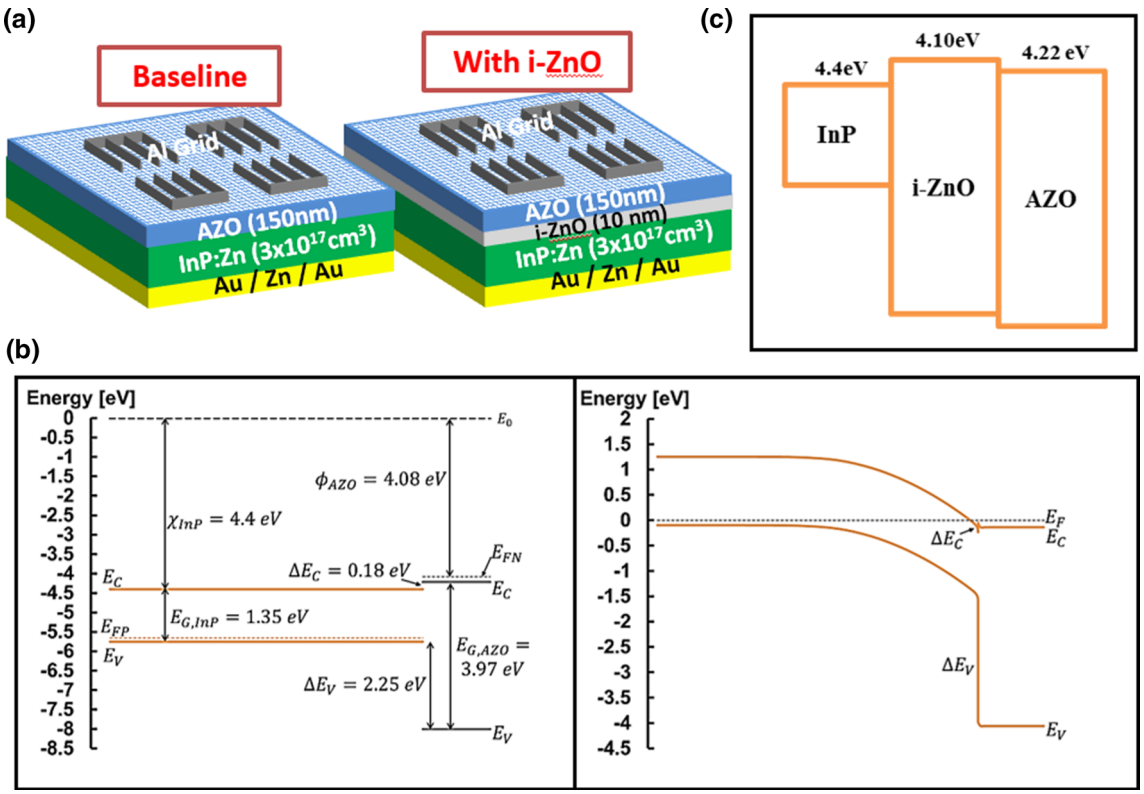

Fig. 1 **a** Schematic overview of the devices used in this study. "Baseline" device consisted of a single film of AZO on an InP:Zn substrate. The "with i-ZnO" device has a thin i-ZnO film deposited prior to the AZO film. Energy band diagrams for the AZO/InP heterojunction: **b** Band alignments assuming a Schottky model showing a type II heterojunction with small conduction band offset relative to the large valence band offset; **c** Equilibrium band diagram with doping levels for devices investigated, assuming no interface recombination centers. **d** Band alignments with i-ZnO interlayer between AZO emitter and InP base, showing enlarged conduction band offset

enlarged conduction band offset is beneficial for preventing recombination and boosting up conversion efficiency.

3.2 I–V curve and conversion efficiency

Following device fabrication, dark current–voltage (I–V) characterization was conducted in a lighttight enclosure using a Keithley 2400 semiconductor parameter analyzer. A Class AAA AM1.5 solar simulator (Oriel Sol3A) was used for light current–voltage characterization, with the intensity adjusted to the one-sun condition using a calibrated Si solar cell. Current–voltage characteristics, in the dark and under an AM1.5G reference spectrum, are shown in Fig. 2 for each of the devices (baseline and with i-ZnO samples). Figure 2a represents linear plot of dark current as a function of bias voltage, with a semilog scale plot insert. Both baseline and with i-ZnO devices exhibited rectifying characteristic with reverse saturation current density, J_0, on the order of 10^{-10} A/cm^2. Ideality factor, determined by the slope of the curve under moderate forward bias, was typically between 1.1 and 1.35. Series resistance became dominate at larger forward bias (>0.6 V) as shown by the bending over of the forward-bias I–V curve, in which it seems the series resistance of with i-ZnO sample suffers from higher value and might drawback overall conversion performance. However, as demonstrated by light I–V curved collected under illumination (Fig. 2b), open-circuit voltages (V_{oc}) of ~0.55 and ~0.58 V were recorded, with short-circuit current density (J_{sc}) of ~15.4 and ~17.4 mA/cm^2 and fill factor (FF) of 72.1 and 72.9 %, subject to baseline and with i-ZnO device, respectively. No significant degradation due to shunt resistance was observed, in examining the flatness of the light I–V curve near J_{sc}. Series resistance, as indicated by the non-vertical slope of the light I–V curve near V_{oc}, was consistent with the observation in the dark I–V measurement. Comparing performance parameters in Fig. 2b insert of these two devices, we demonstrate that a ~20 % conversion efficiency increase was achieved with i-ZnO implant, implying that the series resistance might not be dominant though brought about by insulator ZnO. On the contrary, this scenario happens demonstrating the statement of preventing electrical inhomogeneities like sites of locally enhanced recombination by i-ZnO, which diminish the

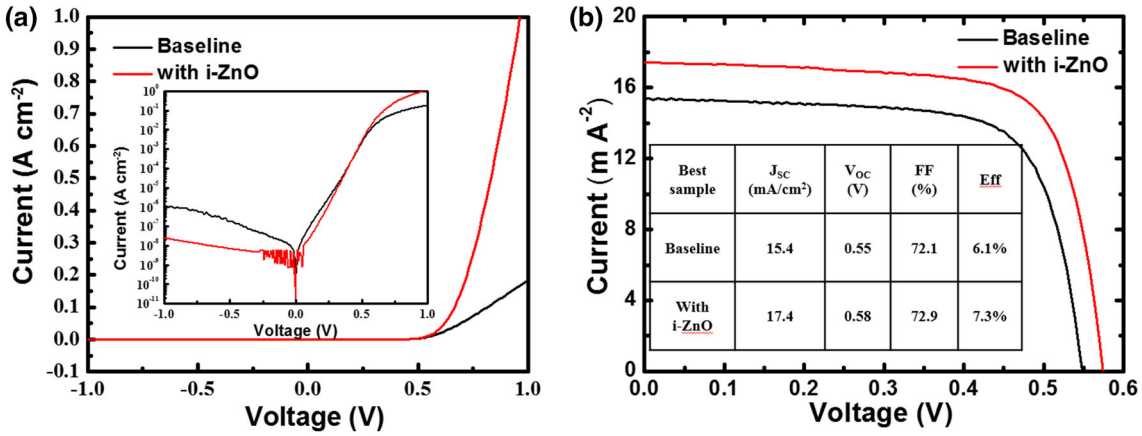

Fig. 2 **a** Dark I–V characteristics from the two representative devices. The "baseline" device exhibited higher reverse saturation current compared to the "with i-ZnO" device. Insert indicates semilog scale plot. **b** I–V characteristics of each device under an AM1.5G solar simulator. In agreement with the dark I–V data, the device with i-ZnO exhibited the highest open-circuit voltage. In addition, it had the highest short-circuit current, yielding an overall efficiency of 7.3 % higher than 6.1 % for baseline. The mesa area of measured devices was 0.0625 cm^2, with grid shadowing loss ~12 %. Insert indicates key parameters related to conversion efficiency. Insert is the diagram of key parameters related with efficiency

Table 1 Summary of electrical properties

	n	J_0 (A/cm^2)	J_{SC} (mA/cm^2)	V_{OC} (V)	FF (%)	η (%)
Baseline	1.34	1.4e−9	15.4	0.55	73	6.1
With i-ZnO	1.26	6.2e−10	17.4	0.57	73	7.3
Pande[a]	1.54	4.0e−8	19.3	0.56	61	6.6

[a] From [10], devices measured under AM 1 reference spectrum and did not include contact grid

base–emitter interface recombination [20, 21] and thus increase carrier collection probability. A summary of key parameters determined from the I–V characteristics for each device is also given in Table 1 and compares with relevant prior ZnO–InP heterojunction device [14]. As indicated by the data in Table 1, the best performing device was the one which incorporated an i-ZnO interlayer between the InP base and the AZO emitter. Of additional interest is that this device represents an improvement (10.5 % increase, relative) over the relevant prior work in the literature, by Pande and Manikopoulos [14]. We believe that the achievement is due to the use of the i-ZnO interlayer, based on the side-by-side comparison between baseline performance and the result of Pande and Manikopulos [14].

3.3 Effect of i-ZnO interlayer

In order to delve into the reason of device performance improvement with i-ZnO interlayer, we investigated the material characteristic difference between AZO layer and with 10 nm i-ZnO buffer in Fig. 3. Prior to full device characterization, several films were characterized on both glass substrates as well as InP. The transmittance was collected by Lambda 950 for AZO film on glass (Fig. 3a) and compared with AZO/i-ZnO counterpart. Field emission scanning electron microscopy (FESEM) was used to determine the thickness of AZO film via cross section (Fig. 3a insert). Sheet resistivity, carrier density, and mobility of the AZO films were deduced from Hall effect measurements using an MMR Technologies K2500 system. A four-point probe was used to verify sheet resistivity. First of all, transmission through AZO films is >85 % from 400 to 1000 nm, as shown in Fig. 3a. However, in our case, transmission is cut off due to the glass substrate; the actual oxide film transmittance should be even higher than 90 % if glass substrate reference were taken off. The lower limit due to absorption in ZnO is around 365 nm. Comparing the transmittance between AZO and AZO/ZnO films, we found the extra 10-nm-thick i-ZnO layer decrease the transmittance in the range of 400–550 nm, while the small fluctuation should not dominate full-cell performance. Figure 3a insert shows the FESEM cross section of oxide layer on InP, which exhibit an ~160-nm-thick zinc oxide layer on top of InP bulk. The PLD accomplished an ultra-flat and uniform oxide layer; however, it is impossible to distinguish between doped ZnO and intrinsic ZnO. Therefore, X-ray diffraction patterns (XRD) were collected for the two compared full devices as shown in Fig. 3b. The three peaks are well indexed to InP (200), ZnO (002), and Al

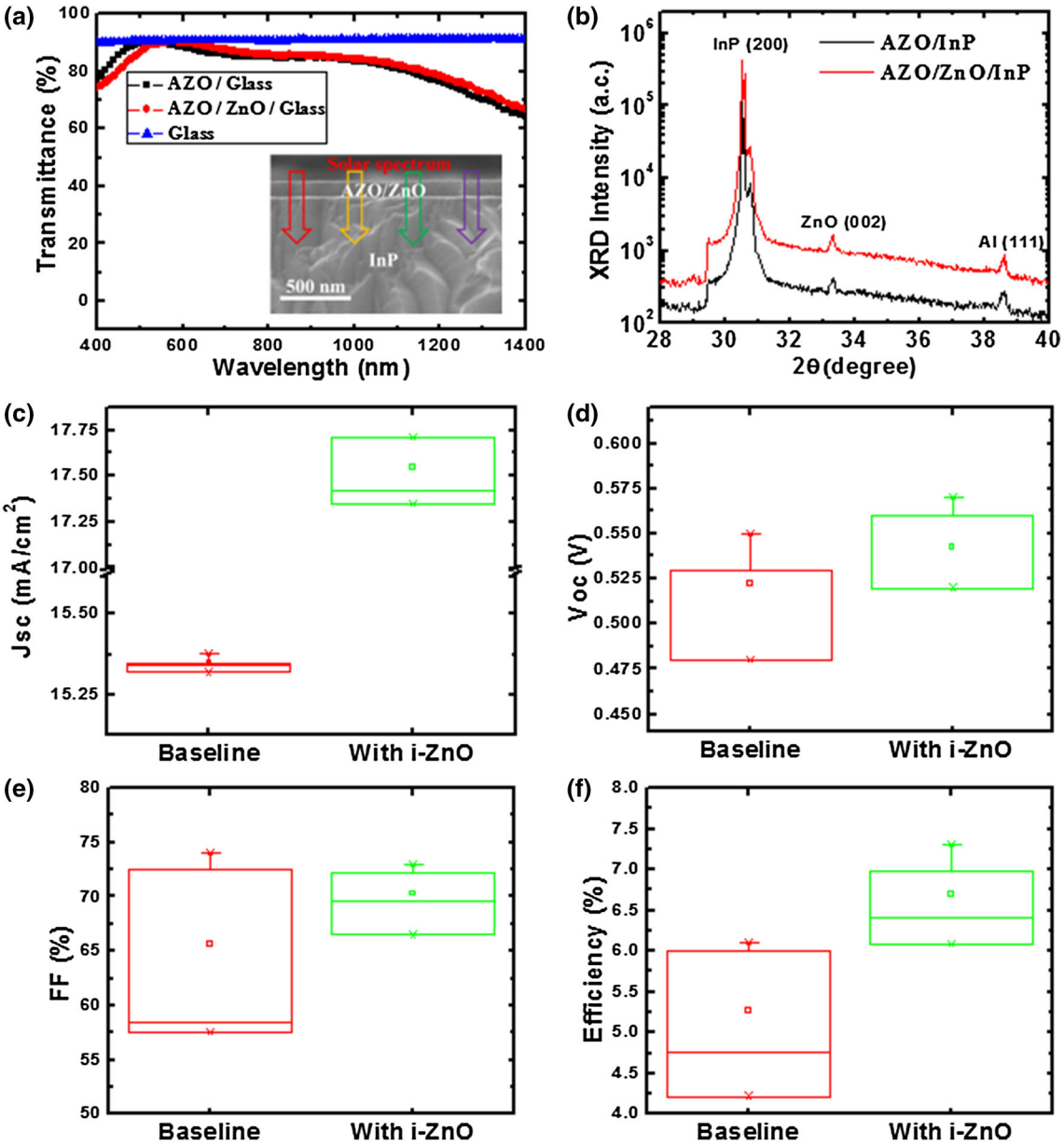

Fig. 3 **a** Transmittance of AZO and AZO/i-ZnO counterpart on glass slides is shown, indicating film transmittance >85 % from 400 to 1000 nm. The insert is FESEM cross-sectional image of AZO/i-ZnO film deposited on InP base. The thickness of metal oxide layer is shown around 160 nm. **b** XRD of baseline devices and the device with i-ZnO. The major peaks are well indexed to InP (200), ZnO (002), and Al (111). Conversion efficiency and dominant factors are compared between baseline cells and i-ZnO cells in box chart: **c** short-circuit current; **d** open-circuit voltage; **e** fill factor; **f** efficiency

(111) in the spectrum. No apparent peak intensity increase was detected for i-ZnO grown beneath AZO, compared with pure AZO grown on InP, implying similar zinc oxide crystal size. Hall effect measurements from representative AZO films yielded a resistivity of 1.6×10^{-3} Ω-cm, with a mobility of 5.8 cm^2/V-s. Carrier density of majority carrier electrons was also measured to be 6.9×10^{20} cm^{-3}. These values are consistent with previous work by PLD of AZO films [26, 30].

Therefore, the further uncertainty drives us to analyze the key parameters statistically such as short-circuit current (J_{SC}), open-circuit voltage (V_{OC}), and fill factor (FF), owning to the theoretical equation of $\eta = V_{OC}J_{SC}A \times \mathrm{FF}/P_{in}$, where A denotes the test area and the P_{in} denotes the input solar power. Figure 3c compares four different devices for each sample (baseline and with i-ZnO) in box chart. It clearly shows higher J_{SC} for cells with i-ZnO interlayer (with a mean of 17.5 mA/cm^2) than baseline

cells (with a mean of 15.3 mA/cm^2). The ~15 % increase factor of J_{SC} has to be ascribed to the collection probability improvement with i-ZnO layer for surface passivation [31], because the testing cells (baseline and with i-ZnO) are side by side measured with the same testing area, solar spectrum, InP base condition, and window layer transmittance (even lower with i-ZnO). Figure 3d compares the V_{OC} as well, exhibiting higher V_{OC} for cells with i-ZnO interlayer for both mean value and best value. The comparison sends a signal of lower recombination rate with i-ZnO layer enlarged conduction band offset [29]. However, the V_{OC} does not boost significantly with i-ZnO interlayer, which is due to the stated optimal value of positive conduction band offset (0.1–0.4 eV) [29]. Figure 3e eventually compares the FF, in which a mean value of 70.2 % was achieved by cells with i-ZnO interlayer, higher than a mean value of 65.6 % subject to baseline cells; however, the peak values of FF do not change much. And it is well known that the FF signals multiple recombination mechanisms, which would be degraded if particularly large recombination mechanisms were achieved [32]. Consequently, Fig. 3f demonstrates that both mean value and peak value of with i-ZnO devices surpass baseline devices.

3.4 Quantum efficiency analysis

In sum of analyzing cell conversion performance with extra i-ZnO interlayer and pure AZO grown on InP, the efficiency improvements with i-ZnO attribute to a ~15 % increase in J_{SC}, a ~5 % increase in V_{OC}, and a ~10 % increase in FF. Moreover, the short-circuit current increase could be ascribed to enhanced collection probability, which further traces to modified surface passivation and lowered surface recombination rate [32], while the open-circuit voltage and fill factor increase mainly result from decreased bulk recombination rate. The bulk recombination rate though depends on InP base material characteristics is also affected by local recombination sites such as grain boundaries and spatial local shunts, which might be prevented by uniformly deposited i-ZnO layer. To further confirm these assumptions, the reflectance, external quantum efficiency (EQE), and internal quantum efficiency (IQE) are measured, as shown in Fig. 4. Reflectance of AZO films on InP was examined using a Lambda 950 UV–Vis–NIR spectrophotometer, which exhibits a typical effect for a quarter wavelength anti-reflection coating, where reflectance is minimized at a single wavelength that corresponds to the film thickness and refractive index. Figure 4 black line shows a minimum reflectance occurred at 730 nm. With a measured refractive index of 1.8, a film thickness of ~100 nm is deduced. Note that final devices were fabricated with AZO thickness of 150 nm, which would shift the minimum reflectance point to around 1080 nm. EQE and IQE were measured by standard techniques using a monochromated Xe arc lamp, optical chopper, and lock-in amplifier. The EQE and IQE for each device are shown in Fig. 4a, b. Integration of the quantum efficiency curves validates the measured J_{sc} values under AM1.5G. The device with i-ZnO showed a clear increase in both EQE and IQE over most of the measured range, compared to the baseline device. In particular, there was a clear distinction in the range of 400–500 nm. All devices displayed a characteristic peak between 400 and 420 nm, before dropping down and leveling off, with an eventual cutoff around 940 nm, which correlates with the band gap of InP.

First, in examining the EQE and IQE data, we find an initial peak between 400 and 420 nm. This is due both to the

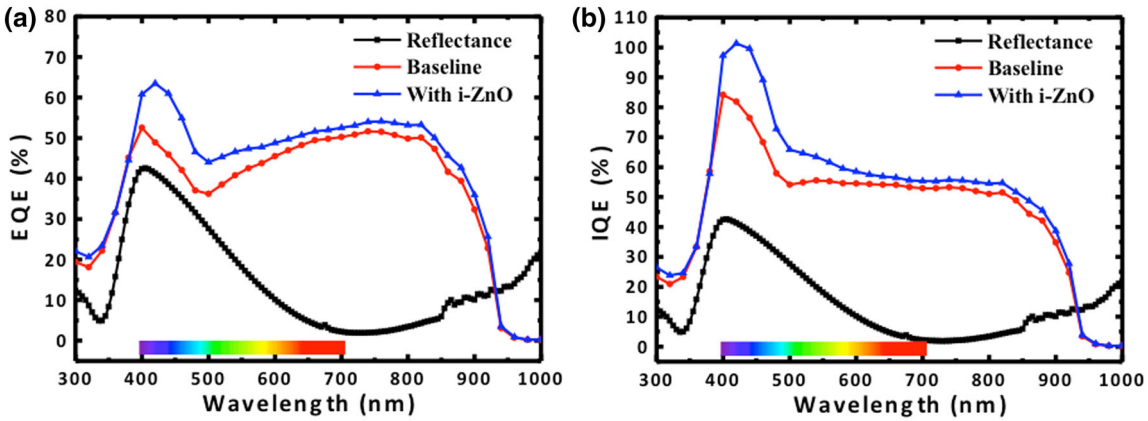

Fig. 4 **a** The absolute external quantum efficiency (EQE) of the fabricated devices is shown. The device with i-ZnO has overall higher quantum efficiency, particularly in the range of 400–600 nm. Reflectance of AZO film on InP substrate is collected with minimum reflectance at 730 nm was measured. **b** The internal quantum efficiency (IQE) of the fabricated devices is shown in the presence and absence of i-ZnO interlayer

sharp reflectance change, but also correlates with the expected depletion region thickness. At an acceptor doping concentration of 3×10^{17} cm^{-3}, the depletion width is approximately 80 nm, assuming a one-sided junction. Correspondingly, the absorption coefficient in InP at 500 nm, where the peak diminishes, is about 1.3×10^5 cm^{-1}, which correlates with an absorption depth of 75 nm. Therefore, what we observe is enhanced quantum efficiency for carriers generated in the depletion region, where the electric field aids in collection. Photons absorbed deeper in the base are limited by diffusion lengths, which are assumed to be relatively short, given that the base is a bulk InP substrate, as opposed to an impurity-free epitaxial film. Note that the gradual increase from 500 to 800 nm is not indicative of the material parameters, but correlates with the change in reflectance, which is decreasing. And this could be demonstrated by slightly decreasing IQE in the wavelength range of 500–800 nm.

Second, the results indicate a clear enhancement in performance of the device with a thin i-ZnO interlayer. In particular, the device with i-ZnO has EQE as much as 10 % (absolute) higher than the baseline device, as well as IQE. This improvement is more significant in the region correlated with absorption in the depletion region, as discussed above, from 400 to 500 nm. Since the quantum efficiency in this region directly signals front surface recombination rate and relates to emitter diffusion length. It is evident that i-ZnO buffer beneath AZO window layer serves to decrease surface recombination rate and enhance collection efficiency. Moreover, the results also indicate a slight enhancement of EQE and IQE for device with i-ZnO in green light region (wavelength range from 500 to 600 nm). It is generally convinced that the green light is absorbed in the bulk of a solar cell and would be affected by multiple recombination rates. This enhancement further verifies that overall device conversion performance has been improved by i-ZnO interlayer. However, while AZO is generally preferred over ZnO due to enhanced carrier concentration and mobility, the underlying mechanisms for transport are not thoroughly understood and need to be investigated further, such as in cases of devices with gradually increasing i-ZnO thickness.

4 Conclusion

In conclusion, we have demonstrated InP/i-ZnO/AZO heterojunction solar cells. A maximum power conversion efficiency of 7.3 % was realized with i-ZnO interlayer, which is $\sim$20 % higher than using pure AZO as the emitter with a best performance of 6.1 %. We have verified that the use of an i-ZnO interlayer between an InP base and AZO emitter has the potential to enhance the collection probability and decrease recombination rate (surface and bulk), which in turn enlarge the short-circuit current, open-circuit voltage, and fill factor. Therefore, in consequence, the device with i-ZnO yields higher solar conversion efficiency, EQE and IQE over a baseline AZO/InP device. The superiorities with using i-ZnO might be able to ascribe to two hypothesis: (1) carrier collection probability enhancement due to surface passivation and base–emitter interface recombination rate decrease; (2) recombination rates lowering due to decreased recombination sites such as InP base grain boundaries and spatial locally shunts, which result from uniformly coated highly resistive ZnO interlayer and enlarged conduction band offset.

References

1. C.H. Henry, J. Appl. Phys. **51**, 4494 (1980)
2. S. Adachi, J. Appl. Phys. **66**, 6030 (1989)
3. S.Y. Prislopski, I.M. Tiginyanu, L. Ghimpu, E. Monaico, L. Sirbu, S.V. Gaponenko, Appl. Phys. A **117**, 467 (2014)
4. Y. Sun, J.M. Woodall, J.L. Freeout, R.J. Walters, Presented at the Photovoltaic Specialists Conference, 2002. Conference Record of the Twenty-Ninth IEEE, 2002 (unpublished)
5. X. Li, M.W. Wanlass, T.A. Gessert, K.A. Emery, T.J. Coutts, Appl. Phys. Lett. **54**, 2674 (1989)
6. K.S.S. Harsha, K.J. Bachmann, P.H. Schmidt, E.G. Spencer, F.A. Thiel, Appl. Phys. Lett. **30**, 645 (1977)
7. M.J. Tsai, A.L. Fahrenbruch, R.H. Bube, J. Appl. Phys. **51**, 2696 (1980)
8. Q.X. Jia, J.P. Zheng, H.S. Kwok, W.A. Anderson, Thin Solid Films **258**, 260 (1995)
9. T.A. Gessert, X. Li, M.W. Wanlass, A.J. Nelson, T.J. Coutts, J. Vac. Sci. Technol. A **8**, 1912 (1990)
10. X. Yin, C. Battaglia, Y. Lin, K. Chen, M. Hettick, M. Zheng, C.-Y. Chen, D. Kiriya, A. Javey, ACS Photon. **1**, 1245 (2014)
11. S. Saito, Y. Hashimoto, K. Ito, Presented at the Photovoltaic Energy Conversion, 1994. Conference Record of the Twenty Fourth. IEEE Photovoltaic Specialists Conference—1994, 1994 IEEE First World Conference on, 1994 (unpublished)
12. C.J. Keavney, V.E. Haven, S.M. Vernon, Presented at the Photovoltaic Specialists Conference, 1990. Conference Record of the Twenty First IEEE, 1990 (unpublished)
13. M. Purica, E. Rusu, E. Budianu, S. Nan, Presented at the Semiconductor Conference, 1998. CAS '98 Proceedings. 1998 International, 1998 (unpublished)
14. K.P. Pande, C.N. Manikopoulos, Solar Cells **4**, 147 (1981)
15. M. Ivill, M. Patel, K. Kim, H. Bae, S.J. Pearton, D.P. Norton, J.D. Budai, Appl. Phys. A **75**, 699 (2002)
16. A.H. Jahagirdar, A.A. Kadam, N.G. Dhere, Presented at the Photovoltaic Energy Conversion, Conference Record of the 2006 IEEE 4th World Conference on, 2006 (unpublished)
17. S. Ishizuka, K. Sakurai, A. Yamada, K. Matsubara, P. Fons, K. Iwata, S. Nakamura, Y. Kimura, T. Baba, H. Nakanishi, T. Kojima, S. Niki, Sol. Energy Mater. Sol. Cells **87**, 541 (2005)
18. K. Ottosson, *The role of i-ZnO for shunt prevention in Cu(In, Ga)Se2-based solar cells* (Uppsala Universitet, Uppsala, 2006)
19. R. Scheer, L. Messmann-Vera, R. Klenk, H.W. Schock, Prog. Photovolt. Res. Appl. **20**, 619 (2012)
20. U. Rau, M. Schmidt, Thin Solid Films **387**, 141 (2001)

21. U. Rau, P.O. Grabitz, J.H. Werner, Appl. Phys. Lett. **85**, 6010 (2004)
22. A. Jahagirdar, A. Kadam, N. Dhere, in *Conference Record of the 2006 IEEE 4th World Conference on Photovoltaic Energy Conversion* (Waikoloa, Hawaii, 2006), pp. 557
23. L. Burstein, J. Bregman, Y. Shapira, J. Appl. Phys. **69**, 2312 (1991)
24. T.E. Fischer, Phys. Rev. **142**, 519 (1966)
25. P. Sang-Moo, I. Tomoaki, E. Kenji, Jpn. J. Appl. Phys. **45**, 8453 (2006)
26. M.Y. Zhang, G.J. Cheng, Appl. Phys. Lett. **99**, 051904 (2011)
27. I. Lange, S. Reiter, M. Pätzel, A. Zykov, A. Nefedov, J. Hildebrandt, S. Hecht, S. Kowarik, C. Wöll, G. Heimel, D. Neher, Adv. Funct. Mater. **24**, 7014 (2014)
28. L. Weinhardt, C. Heske, E. Umbach, T.P. Niesen, S. Visbeck, F. Karg, Appl. Phys. Lett. **84**, 3175 (2004)
29. F.S. Hasoon, H.A. Al-Thani, L. Xiaonan, A. Kanevce, C. Perkins, S. Asher, Presented at the Photovoltaic Specialists Conference, 2008. PVSC '08. 33rd IEEE, 2008 (unpublished)
30. Q. Nian, M.Y. Zhang, B.D. Schwartz, G.J. Cheng, Appl. Phys. Lett. **104**, 201907 (2014)
31. A.J. McEvoy, T. Markvart, L. Castañer, *Practical Handbook of Photovoltaics: Fundamentals and Applications* (Academic Press, Waltham, 2012)
32. M.A. Green, Solid State Electron. **24**, 788 (1981)